

Optical and near-IR photometric study of the open cluster NGC 637 and NGC 957

R. K. S. Yadav^{1*}, Brijesh Kumar^{1,2}, A. Subramaniam³, Ram Sagar¹ and Blesson Mathew³

¹ *Aryabhata Research Institute of Observational Sciences, Manora Peak, Nainital 263129, India*

² *Departamento de Física, Universidad de Concepción, Casilla 160-C, Concepción, Chile*

³ *Indian Institute of Astrophysics, Bangalore 560 034, India*

6 November 2018

ABSTRACT

We present *UBVRI* CCD photometry in the region of the open clusters NGC 637 and NGC 957. The radii are found to be $4'.2$ and $4'.3$. Their reddenings $E(B - V)$ are 0.64 ± 0.05 mag and 0.71 ± 0.05 mag and their distances, from main sequence fitting are 2.5 ± 0.2 kpc and 2.2 ± 0.2 kpc. Comparison with $Z = 0.02$ isochrones leads to an age of 10 ± 5 Myr for both clusters. Combining our photometry with 2MASS JHK shows the reddening law in these directions to be normal. Mass function slopes of $x = 1.65 \pm 0.20$ and 1.31 ± 0.50 are derived for the clusters, both of which are found to be dynamically relaxed. Spectral and photometric characteristics of three Be stars, two in NGC 957 and one (newly discovered) in NGC 637 indicate them to be of Classical Be type.”

Key words: Key words: stars: emission-line, Be HertzsprungRussell (HR) diagram stars: luminosity function, mass function ISM: dust, extinction Galaxy: open cluster and associations: individual: NGC 637 and NGC 957.

1 INTRODUCTION

Open clusters are excellent targets to understand issues related to Galactic structure, chemical composition, stellar population, dynamical evolution and star formation processes in the Galaxy. The importance of photometric studies of star clusters lie in their colour-magnitude diagrams (CMDs) which allow us to estimate cluster’s fundamental parameters such as age, distance and reddening. In this study, we consider two young open cluster, NGC 637 and NGC 957, situated in perseus arm of Milky Way to estimate their fundamental parameters and mass function.

NGC 637 = C0139+637 ($\alpha_{2000} = 01^h 43^m 04^s$, $\delta_{2000} = +64^\circ 02' 24''$; $l = 128^\circ 55'$, $b = 1^\circ 73'$) is classified as a Trumpler class I2m by Ruprecht (1966). Using *RGU* photographic data, Grubisich (1975) found the cluster to be located in the Perseus arm at a distance of 2.4 kpc. Huestamendia et al. (1991) used the *UBV* photoelectric photometry and derived a colour excess of $E(B - V) = 0.66$ mag and a distance of 2.5 kpc. Recently, Phelps & Janes (1994) studied this cluster using *UBV* CCD photometry and estimated a colour excess of $E(B - V) = 0.49 \pm 0.03$ mag. Further, using CMD and assuming a total-to-selective absorption (R_V) of 3.1, they derived a distance of 2.75 kpc.

NGC 957 = C0230+573 ($\alpha_{2000} = 02^h 33^m 21^s$, $\delta_{2000} = 57^\circ 33' 36''$; $l = 136^\circ 28'$, $b = -2^\circ 65'$) is located in the Perseus spiral arm of our Galaxy and according to Ruprecht (1966), it is of type III 2p. This cluster was studied by Gimenez & Garcia-pelayo (1980) using *RGU* photographic photometry and they found that this is an young star cluster situated at a distance of 1.8 kpc. This cluster was further investigated by Gerasimenko (1991) using Johnson *UBV* photoelectric and photographic photometry. He derived reddening of $E(B - V) = 0.90$ mag, distance of 2.1 kpc and age of about 4 Myr.

In the present study, we provide deep *UBVRI* CCD photometry of NGC 637 and NGC 957, and re-visit their basic parameters and estimate their luminosity and mass functions. Both the clusters are poorly studied in the literature. For NGC 957, CCD photometric observations is presented for the first time alongwith spectroscopic observations of a few brightest members of both the clusters.

The paper is organized as follows. We present the observations and data reductions in §2, while in §3, we describe the data analysis. §4 and §5 describe about the mass function and mass segregation. Finally, §6 contains the conclusions of our study.

* E-mail: rkant@aries.ernet.in

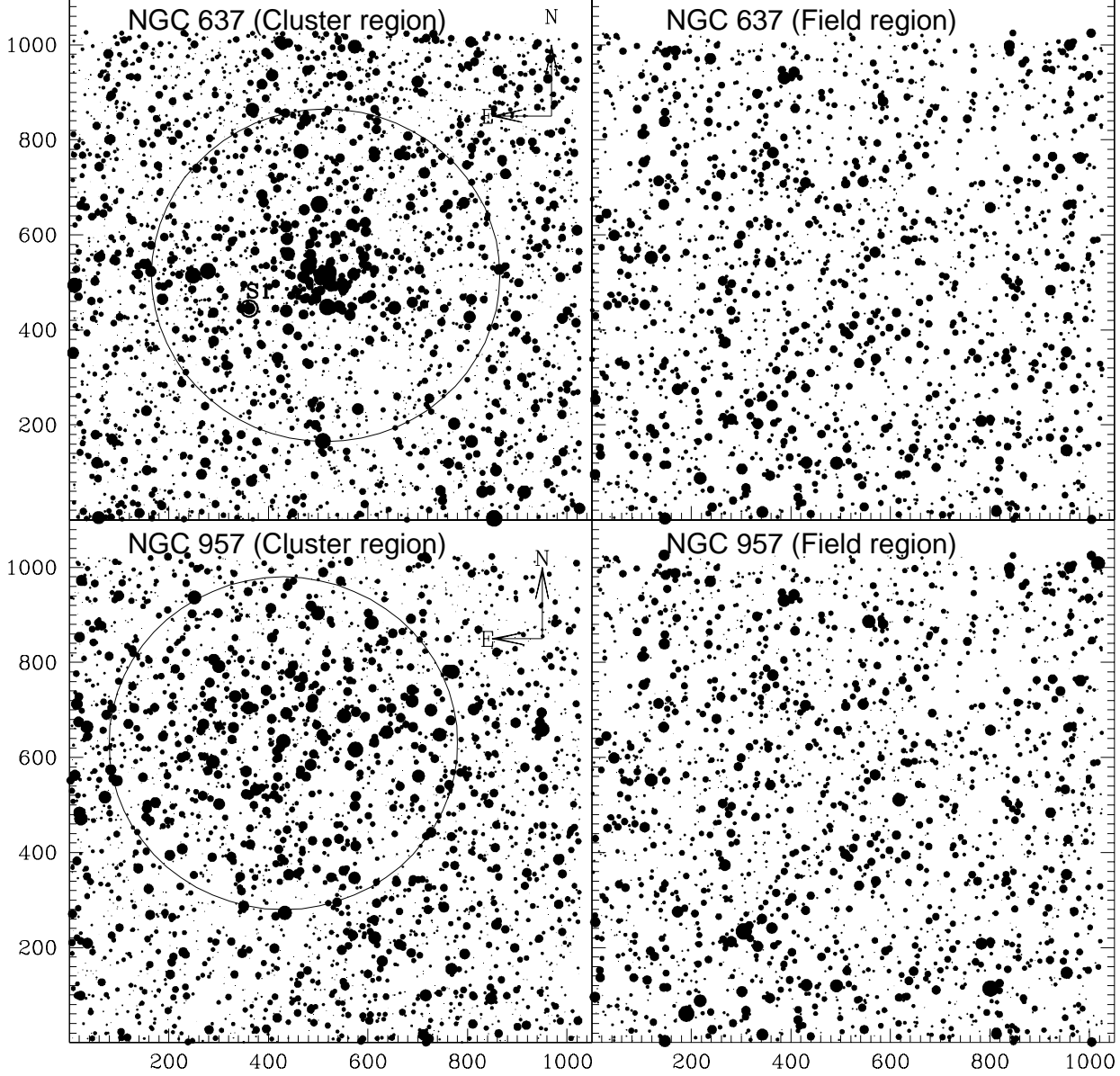


Figure 1. Finding chart of the stars in the field of NGC 637 and NGC 957. The (X, Y) coordinates are in pixel units corresponding to $0''.72$ on the sky. Direction is indicated in the map. Filled circles of different sizes represent brightness of the stars. Smallest size denotes stars of $V \sim 20$ mag. Open circle represent the cluster size. S1 star in the region of NGC 637 is emission type star.

2 OBSERVATIONS AND DATA REDUCTION

2.1 Photometric observations

Johnson *UBV* and Cousins *RI* CCD photometric observations were obtained using 104-cm Sampurnanand telescope at Nainital on 13 November 2004 for NGC 637 and on 28 September 2006 for NGC 957. Data were recorded using a liquid nitrogen cooled $2k \times 2k$ CCD of $24\mu m$ square size pixel, which results in a scale of $0''.36$ per pixel and a square field of $12'.7$ in the sky on a side. The CCD has a gain of

10 electrons per analog-to-digital unit and a read out noise of 5.3 electrons. To improve the signal-to-noise ratio, all the observations were taken in 2×2 binning mode. Log of observations are given in Table 1. In *V* and *I* filters, we also observed field regions situated about $15'$ north from the cluster center of both NGC 637 and NGC 957. Identification maps of cluster and field regions are shown in Fig. 1.

A number of bias and flat-field frames were taken during the observations. Flat-field exposures were taken of the twilight sky in each filter. Bias and flat field corrections were

Table 1. Log of observations, with dates and exposure times for each passband. N denotes the number of stars measured in different passband.

Band	Exposure Time (in seconds)	Date	N
NGC 637(Cluster region)			
U	1800×2, 300×1	2004 November 13/14	1057
B	1200×3, 300×1	2004 November 13/14	
	120×1; 10×1	2004 November 13/14	2392
V	900×3, 120×1; 10×1	2004 November 13/14	3261
R	480×3, 60×2; 5×1	2004 November 13/14	3219
I	300×3, 60×1; 5×1	2004 November 13/14	3151
NGC 637(Field region)			
V	180×2	2004 November 14/15	1286
I	180×2	2004 November 14/15	1266
NGC 957			
U	1800×2, 300×1	2006 September 28/29	915
B	1200×2, 300×2	2006 September 28/29	2087
V	900×2, 180×2	2006 September 28/29	2855
R	600×2, 120×2	2006 September 28/29	2819
I	300×3, 60×2	2006 September 28/29	2707
NGC 957(Field region)			
V	180×2	2004 November 14/15	1284
I	180×2	2004 November 14/15	1269

performed using the standard IRAF¹ tasks. Subsequent data reduction and analysis were done using the DAOPHOT software (Stetson 1987, 1992). We performed the profile fitting photometry using quadratically varying point spread function. For each filter, the stars have been aligned to that of a reference frame with largest exposure time and an average instrumental magnitude weighted by the photometric error was derived. A final catalogue was created of stellar objects identified in at least two filters, with shape-defining parameter $-2 \leq \text{sharpness} \leq 2$ and the goodness-of-fit estimator $\chi \leq 5$.

For translating the instrumental magnitude to the standard magnitude, we observed the standard field PG 0231+051 (Landolt 1992) on 20 November 2004 several times during the night to determine the Earth's atmospheric extinction coefficients, color coefficients and the zero points of the telescope and CCD system. The standard stars used in the calibrations have brightness range of $12.77 \leq V \leq 16.11$ and a color range of $-0.329 < (B-V) < 1.448$. The transformation equations derived using linear least square regression are as follows:

$$\begin{aligned}
 u &= U + 6.92 \pm 0.01 - (0.06 \pm 0.01)(U-B) + (0.54 \pm 0.02)X \\
 b &= B + 4.66 \pm 0.01 - (0.02 \pm 0.01)(B-V) + (0.24 \pm 0.01)X \\
 v &= V + 4.22 \pm 0.01 - (0.01 \pm 0.01)(B-V) + (0.14 \pm 0.01)X \\
 r &= R + 4.13 \pm 0.01 - (0.00 \pm 0.01)(V-R) + (0.10 \pm 0.01)X \\
 i &= I + 4.60 \pm 0.01 - (0.02 \pm 0.02)(R-I) + (0.06 \pm 0.01)X
 \end{aligned}$$

where u, b, v, r and i are the aperture instrumental magnitudes and U, B, V, R and I are the standard magnitudes and X is the airmass. Zero-point and colour-coefficient errors are ~ 0.01 mag.

The internal errors, as derived from DAOPHOT, in magnitude and colour are plotted against V magnitude in Fig. 2. This figure shows that photometric error is ≤ 0.01

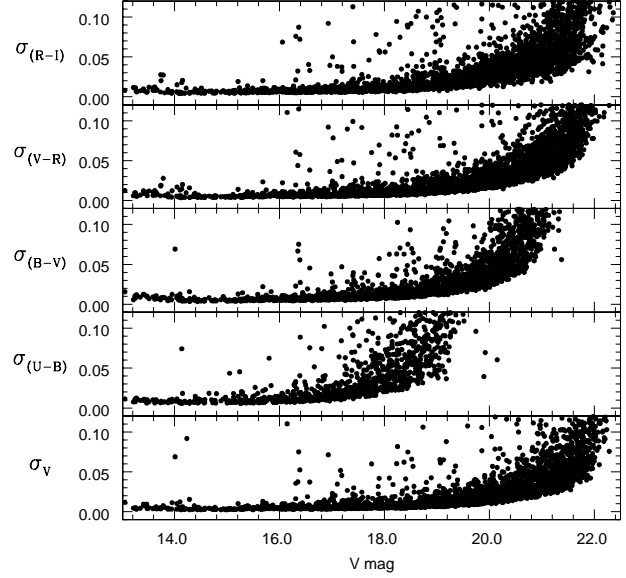


Figure 2. The photometric errors (in magnitude) corresponding to the brightness measurement at V , $U-B$, $B-V$, $V-R$ and $V-I$, are plotted against the V -band brightness. Errors on the y-axis represent the internal errors as estimated by DAOPHOT routine.

Table 2. Comparison of our photometry with others for NGC 637 and NGC 957. The difference (Δ) is always in the sense present minus comparison data. The mean along with their standard deviations in magnitude are based on N stars. Few deviated points are not included in the average determination.

V range	$\langle \Delta V \rangle$ Mean $\pm \sigma(N)$	$\langle \Delta(B-V) \rangle$ Mean $\pm \sigma(N)$	$\langle \Delta(U-B) \rangle$ Mean $\pm \sigma(N)$
NGC 637			
Comparison with Huestamendia et al. (1991)			
10.0 – 11.0	0.01 \pm 0.01(2)	0.01 \pm 0.01(2)	0.02 \pm 0.02(2)
12.0 – 13.0	0.03 \pm 0.05(3)	0.01 \pm 0.01(3)	0.03 \pm 0.02(3)
13.0 – 14.0	0.05 \pm 0.04(8)	0.01 \pm 0.02(8)	0.03 \pm 0.04(8)
14.0 – 15.0	0.02 \pm 0.02(7)	0.01 \pm 0.01(7)	0.04 \pm 0.02(4)
Comparison with Phelps & Janes (1994)			
10.0 – 11.0	0.05 \pm 0.06(4)		
12.0 – 13.0	0.05 \pm 0.04(2)	0.03 \pm 0.01(3)	0.13 \pm 0.03(3)
13.0 – 14.0	0.08 \pm 0.06(12)	0.02 \pm 0.04(14)	0.13 \pm 0.06(14)
14.0 – 15.0	0.06 \pm 0.07(13)	0.03 \pm 0.03(15)	0.14 \pm 0.08(14)
15.0 – 16.0	0.04 \pm 0.04(12)	0.01 \pm 0.05(21)	0.13 \pm 0.05(15)
16.0 – 17.0	0.03 \pm 0.04(44)	0.02 \pm 0.04(45)	0.12 \pm 0.06(27)
17.0 – 18.0	0.03 \pm 0.05(61)	0.01 \pm 0.05(65)	0.10 \pm 0.07(42)
18.0 – 19.0	0.03 \pm 0.08(67)	0.01 \pm 0.06(73)	0.11 \pm 0.08(27)
19.0 – 20.0	0.03 \pm 0.07(102)	0.01 \pm 0.09(96)	
NGC 957			
Comp. with Gimenez & Garcia-pelayo (1980)			
12.0 – 13.0	-0.06 \pm 0.09(5)	-0.03 \pm 0.05(5)	0.03 \pm 0.05(5)
13.0 – 14.0	-0.04 \pm 0.07(6)	-0.03 \pm 0.06(6)	0.03 \pm 0.06(6)
14.0 – 15.0	-0.03 \pm 0.06(3)	-0.03 \pm 0.06(3)	0.03 \pm 0.06(3)

¹ IRAF is distributed by the National Optical Astronomical Observatory which are operated by the Association of Universities for Research in Astronomy, under contract with the National Science Foundation

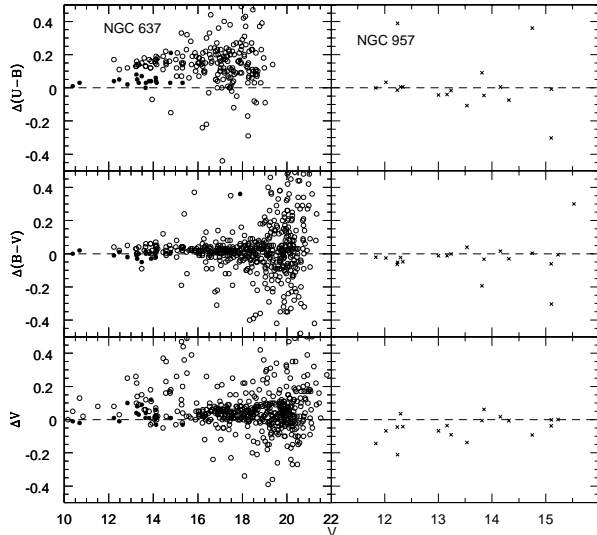


Figure 3. Comparison of present CCD *UBV* photometry with that available in the literature. For NGC 637, the solid (●) circles represent data from Huestamendia et al. (1991) while the open circles (○) come from Phelps & Janes (1994). For NGC 957, the crosses (×) represent comparison with photographic data taken from Gerasimenko (1991).

mag at $V \sim 19$ mag while error in different colours is ≤ 0.02 mag. The final photometric data are available in electronic form at the WEBDA site ² and it can also be obtained from the authors.

We cross identified our objects with that present in the literature. Fig. 3 shows the plots of difference Δ in V , $(B-V)$ and $(U-B)$ with V magnitude. Solid and open circles represent the difference with photoelectric and CCD data. The average difference alongwith their standard deviation are listed in Table 2. The comparison of present and photoelectric data in V magnitude and $(B-V)$, $(U-B)$ colours in NGC 637 do not show any significant difference with stellar magnitudes. Comparison of NGC 957 CCD data with photographic data also do not show any significant difference. So, we conclude that the present CCD photometry is in good agreement with photoelectric and photographic data for NGC 637 and NGC 957 respectively. On the other hand for NGC 637, comparison of CCD data with Phelps & Janes (1994) show a zero-point offset of ~ 0.04 mag in V and ~ 0.12 mag in $(U-B)$ while there is no noticeable difference seen in $(B-V)$. A possible cause of the zero-point offset may be due to the difference in dates of observation for Landolt (1992) standards and the target cluster fields. Since the zero-points depend on the factors, such as ambient temperature and Earth's atmospheric conditions, these coefficients change from night-to-night. A typical nightly variation in zero-points is found to be ~ 0.08 mag in U and ~ 0.05 mag in B, V, R and I passband. In addition to this ~ 0.02 mag nightly variation is found in the extinction coefficients.

Table 3. Log of slitless and slit spectroscopic observations, with dates and exposure times.

Object	Band	Exposure Time (s)	Date
NGC 637	R	5	2004 January 28
	R+Gr5	60	2004 January 28
	R+Gr5	600	2004 January 28
NGC 957(East)	R	5	2004 January 29
	R+Gr5	60	2004 January 29
	R+Gr5	600	2004 January 29
NGC 957(West)	R	5	2004 January 29
	R+Gr5	60	2004 January 29
	R+Gr5	600	2004 January 29
NGC 957(West)	R	5	2004 January 29
	R+Gr5	60	2004 January 29
	R+Gr5	600	2004 January 29
NGC 637(1)	Grism 7/167l	900	2006 September 30
	Grism 8/167l	900	2006 September 30
	Grism 7/167l	300	2006 September 30
NGC 957(1)	Grism 7/167l	300	2006 September 30
	Grism 8/167l	300	2006 September 30
	Grism 7/167l	600	2006 September 30
NGC 957(2)	Grism 7/167l	600	2006 September 30
	Grism 8/167l	600	2006 September 30
	Grism 8/167l	600	2006 September 30

2.2 Spectroscopic observations

We obtained slitless spectra of stars in the cluster regions using Himalayan Faint Object Spectrograph and Camera mounted with the 2-m Himalayan Chandra Telescope at Hanle, India³. Grism 5 ($\lambda \sim 5200 - 10300 \text{ \AA}$, $\lambda/\Delta\lambda \sim 870$) was used as dispersing element in combination with R filter ($\lambda \sim 7000 \text{ \AA}$, $\Delta\lambda \sim 2200 \text{ \AA}$). The slitless spectra were recorded on a $2k \times 2k$ CCD with $15\mu\text{m}$ pixel size and with an image scale of $0''.297$ per pixel, which covered a total area of around $10' \times 10'$. A typical spectral resolution of 6 \AA is achieved at H_{α} . We list the log of observations in Table 3. We obtained the slit spectra of the three identified emission line stars on 30 September 2006 using Grism 7 ($3800 - 6800 \text{ \AA}$) and $167 \mu\text{m}$ slit combination in the blue region which gives an effective resolution of 1330. The spectra in the red region were obtained on the same night using Grism 8 ($5800 - 8350 \text{ \AA}$) and $167 \mu\text{m}$ slit, which gives an effective resolution of 2190. The Gaussian FWHM seeing was about $1''.5$ (~ 5 pixel).

3 ANALYSIS OF THE DATA

3.1 Cluster radius and radial stellar surface density

We perform star counts in concentric rings around an estimated centre of the cluster, and then divide it by their respective areas. The cluster center is estimated iteratively by calculating average X and Y position of the stars within 400 pixels from an eye estimated center, until they converged to a constant value. The cluster center in pixel units derived by this method are (515, 515) for NGC 637 and (430, 630) for NGC 957. The cluster center in celestial coordinate are ($\alpha_{2000} = 01^h 43^m 04^s.2$, $\delta_{2000} = 64^{\circ} 02' 23''.5$) for NGC 637 and ($\alpha_{2000} = 02^h 33^m 23^s.9$, $\delta_{2000} = 57^{\circ} 33' 29''.9$) for NGC 957. The derived center of both the clusters are close to the one given in WEBDA (§1). In Fig. 4 we show the radial

² <http://obswww.unige.ch/webda/>

³ <http://www.iia.res.in>

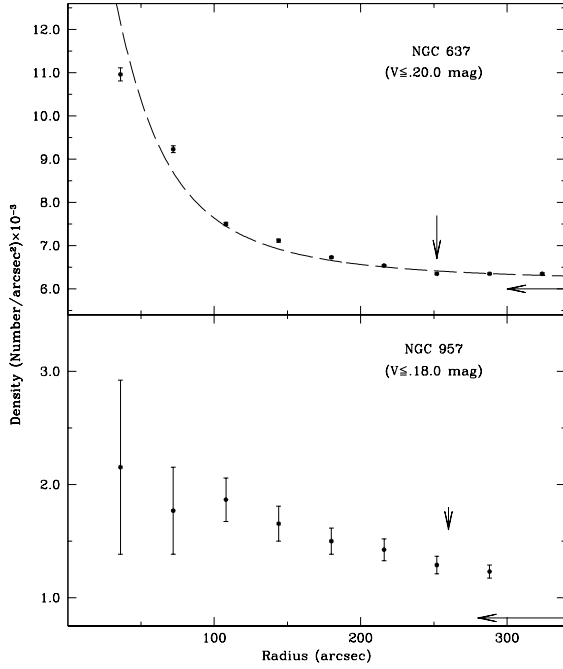


Figure 4. Surface density distribution of stars in the field of the cluster NGC 637 and NGC 957. Errors are determined from sampling statistics ($=1/\sqrt{N}$ where N is the number of stars used in the density estimation at that point). Vertical and horizontal arrows represent the radius of the clusters and field star density respectively.

density profile for both the clusters which is calculated using successive annuli of 50 pixels ($\sim 35''$) around the cluster centre. For NGC 637, it flattens around $r = 250''$ and begin to merge with the background stellar density. Therefore, we consider $250''$ as the cluster radius. A smooth dashed line represents a fit by King (1962) profile:

$$f(r) = \frac{f_0}{1 + (r/r_c)^2} + f_b \quad (1)$$

where f_0 is the central density, r_c is the core radius of the cluster and f_b is the background density. For NGC 637, these parameters are $f_0 = 10.96 \times 10^{-3}$ star/arcsec², $r_c = 39''.6$ and $f_b = 6.15 \times 10^{-3}$ star/arcsec². In case of NGC 957, King (1962) profile fitting could not converge because of large errors in the value of $f(r)$. Radius of this cluster is assumed as $260''$ considering the field star density on the basis of last two points in the radial density profile. For NGC 637 and NGC 957, the radius has been listed as $100''$ and $300''$ in Dias et al. (2002) catalog. Present estimate of the radius is larger for the cluster NGC 637 while it is smaller for NGC 957.

3.2 Colour-magnitude diagrams

The V , $(U-B)$; V , $(B-V)$ and V , $(V-I)$ CMDs of NGC 637 and NGC 957 alongwith the V , $(V-I)$ CMD of the corresponding field regions are shown in Fig. 5. To get the clear sequence of the cluster we plot only the stars within the cluster radius. It is evident that the morphology of CMDs for NGC 637 and NGC 957 is typical of a young age open star clusters. The CMDs extends down to $V \sim 21.0$ mag

except in V , $(U-B)$ CMDs where it is only up to $V \sim 19$ mag. Main-sequence (MS) of the clusters is clearly visible upto $V \sim 17.0$ mag. The MS fainter than 17.0 mag has more scatter and field star contamination is also more evident for fainter stars and because of this it is hard to delineate the field stars from the cluster members, only on the basis of their closeness to the main populated area of the CMD as field stars at cluster distance and reddening also occupy the same area. Proper motion or radial velocity data are very useful in separating cluster members from the field stars. But due to unavailability of this kind of data in the literature we use photometric criterion to separate probable cluster members from the field stars. We selected members by defining the blue and red envelope around the MS which is shown in the CMDs of both the clusters. A star is considered as a non-member if it lies outside the marked region in the CMDs. In Table 4, we have listed the expected number of field stars using V , $(V-I)$ CMD of the field region. From this Table we can estimate the frequency distribution of stars in different parts of the CMD. It is also clear that all photometric probable members cannot be cluster members and non-members should be subtracted in the studies of cluster mass function etc. However, probable members located within a cluster radius can be used to determine the cluster parameters, as they have relatively less contamination due to field stars and the same has been assumed in the subsequent analysis.

3.3 Colour-colour diagram

To estimate the interstellar extinction towards the clusters we plot $(U-B)$ versus $(B-V)$ diagrams using probable cluster members. The intrinsic zero-age main-sequence (ZAMS) given by Schmidt-Kaler (1982) is fitted by the dotted curve assuming the slope of reddening $E(U-B)/E(B-V)$ as 0.72 . The ZAMS fitted to the MS stars of spectral type earlier than A0 provides a mean value of $E(B-V) = 0.64 \pm 0.05$ mag for NGC 637 and $E(B-V) = 0.71 \pm 0.05$ for NGC 957. Our derived values of reddening agree fairly well with the values estimated by others (§1).

3.4 Interstellar extinction in near-IR

2MASS JHK data is used to study the interstellar extinction in combination with the optical data. The K_s magnitude are converted into K magnitude following Persson et al. (1998). The $(J-K)$ versus $(V-K)$ diagrams for both the clusters are shown in Fig. 7. The ZAMS taken from Schaller et al. (1992) for $Z = 0.02$ is shown by solid line. The fit of ZAMS provides $E(J-K) = 0.23 \pm 0.20$ mag and $E(V-K) = 1.70 \pm 0.20$ mag for NGC 637 and $E(J-K) = 0.29 \pm 0.20$ mag and $E(V-K) = 2.00 \pm 0.20$ mag for NGC 957. The ratios $\frac{E(J-K)}{E(V-K)} \sim 0.14 \pm 0.30$ and 0.15 ± 0.20 for NGC 637 and NGC 957 respectively are in good agreement with the normal interstellar extinction value of 0.19 (Cardelli et al. 1989). However, scattering is more due to large error in JHK data.

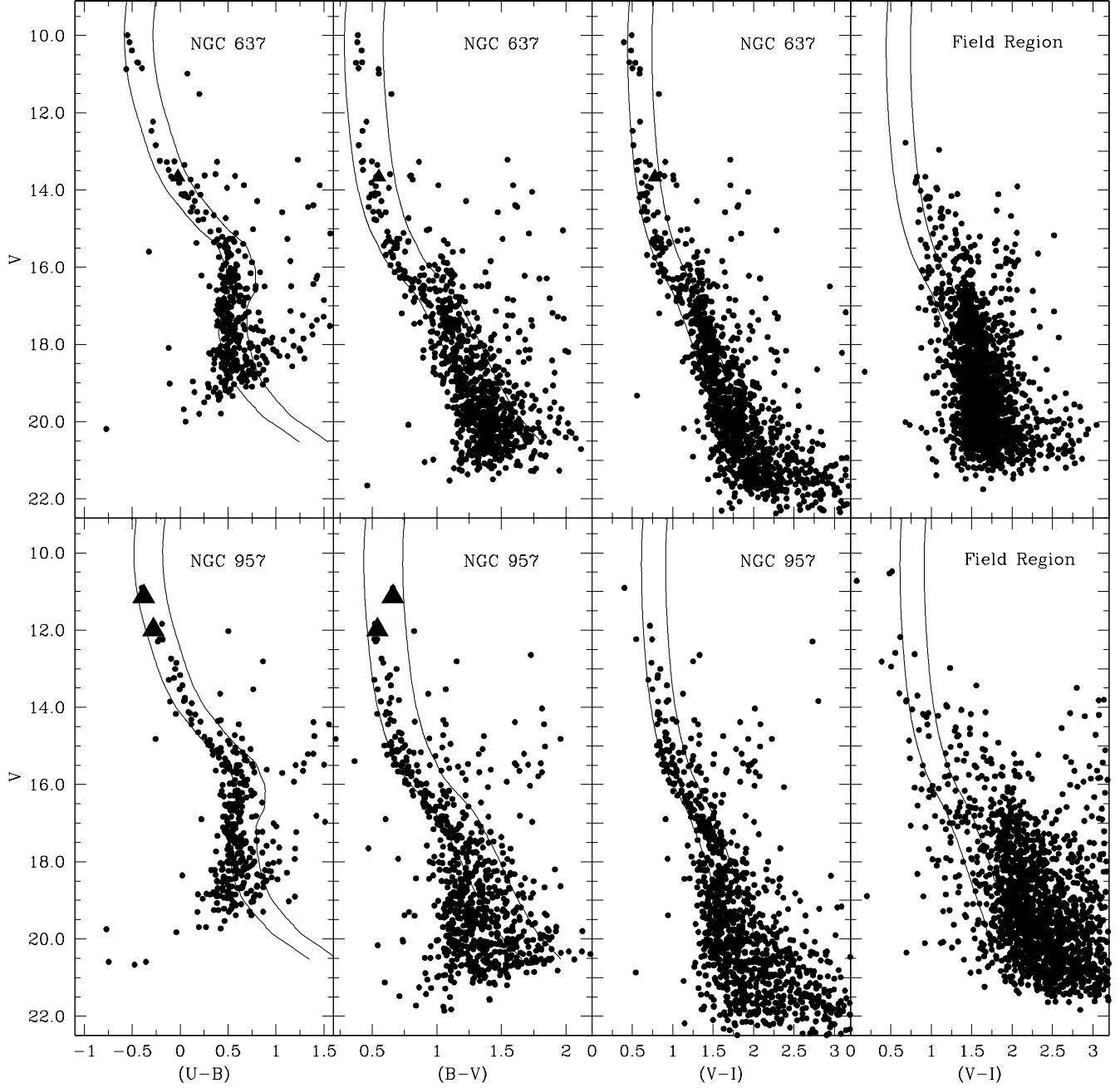


Figure 5. The V , $(U-B)$; V , $(B-V)$ and V , $(V-I)$ CMDs for the cluster NGC 637 and NGC 957 using stars within the cluster radius and V , $(V-I)$ CMDs for the corresponding field regions. Black triangles show the emission stars observed by us. Solid lines represent the blue and red envelope of the cluster MS.

3.5 Extinction Law

To investigate interstellar extinction law towards the clusters under study, we selected stars with spectral type earlier than A0. These have been identified from their location in apparent colour-colour ($U-B$ versus $B-V$) and CM diagrams, having $V < 15$ mag, and $(B-V) < 0.70$ mag, and for these stars, the MS spectral type have been obtained using UBV photometric Q -method (Johnson & Morgan 1953). The colour excesses are determined by subtracting intrinsic

colours from observed colours. The intrinsic colours are derived from the colour relation given by FitzGerald (1970) for $(U-B)$ and $(B-V)$; by Johnson & Morgan (1966) for $(V-R)$ and $(V-I)$ and by Koornneef (1983) for $(V-J)$, $(V-H)$ and $(V-K)$. To get the intrinsic colors for $V-R$ and $V-I$, the present Cousins RI system are converted to the Johnson RI using the relation given by Bessell (1979). Table 5 lists the colour excess ratios estimated for both the clusters alongwith the ratios for normal interstellar matter (Cardelli et al. (1989)). The colour excess ratios generally

Table 4. Frequency distribution of the stars in the V , $(V - I)$ diagram of the cluster and field regions. N_B , N_S and N_R denote the number of stars in a magnitude bin blueward, along and redward of the cluster sequence respectively. The number of stars in the field regions are corrected for area differences. N_C (difference between the N_S value of cluster and field regions) denotes the statistically expected number of cluster members in the corresponding magnitude bin.

V range	NGC 637							NGC 957						
	Cluster region			Field region			N_C	Cluster region			Field region			N_C
	N_B	N_S	N_R	N_B	N_S	N_R		N_B	N_S	N_R	N_B	N_S	N_R	
12 - 13	0	3	0	1	0	0	3	0	2	2	0	0	2	2
13 - 14	10	8	0	5	0	0	8	0	7	4	0	0	5	7
14 - 15	6	15	0	10	0	0	15	0	16	11	0	0	11	16
15 - 16	17	22	0	17	3	0	19	0	35	27	0	0	21	35
16 - 17	40	42	1	28	13	0	29	1	34	20	0	7	38	27
17 - 18	48	62	2	55	24	2	38	3	45	31	2	7	80	38
18 - 19	48	95	4	52	70	5	25	17	66	48	3	26	107	40

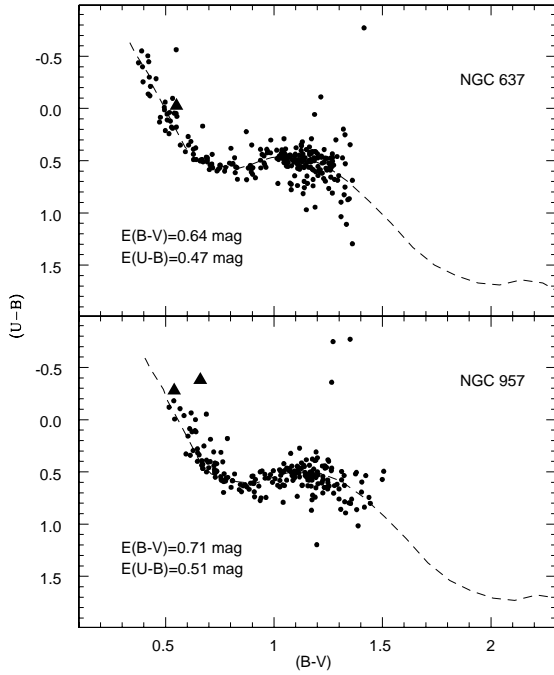


Figure 6. The $(U - B)$ versus $(B - V)$ colour-colour diagram of the clusters. The continuous curve represents locus of Schmidt-Kaler's (1982) ZAMS for solar metallicity. The filled triangles are the emission type stars observed by us.

agree within 3σ with those given for the normal interstellar extinction law. This indicates that the interstellar extinction law is normal in the direction of both the clusters.

Using the relation $R_V = 1.1E(V - K)/E(B - V)$ (Whittet & van Breda 1980), we derived the values of R_V as 3.1 for NGC 637 and 3.2 for NGC 957 and this indicates normal interstellar extinction law in the direction of both the clusters.

3.6 Distance to the clusters

The ZAMS fitting procedure was used to derive distances to the clusters. Fig. 8 shows the intrinsic CMDs of probable cluster members as selected in §3.2 for the clusters NGC 637 and NGC 957. Employing mean $E(B - V)$ for the clusters, we converted apparent magnitude and colours into the intrinsic

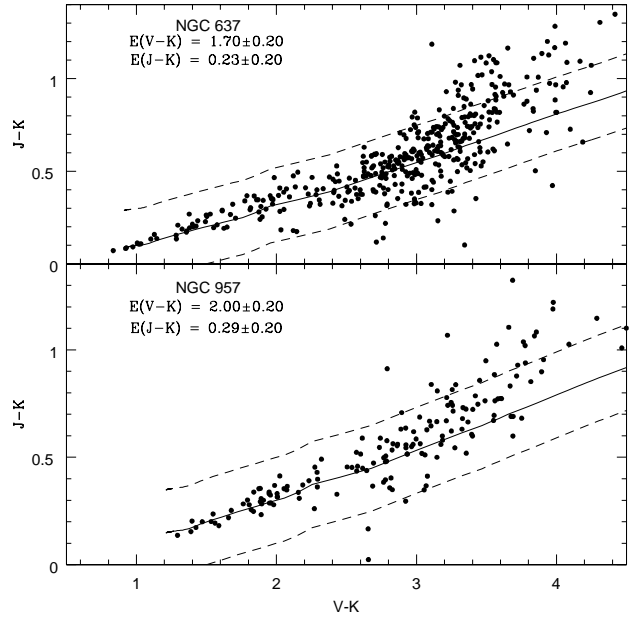
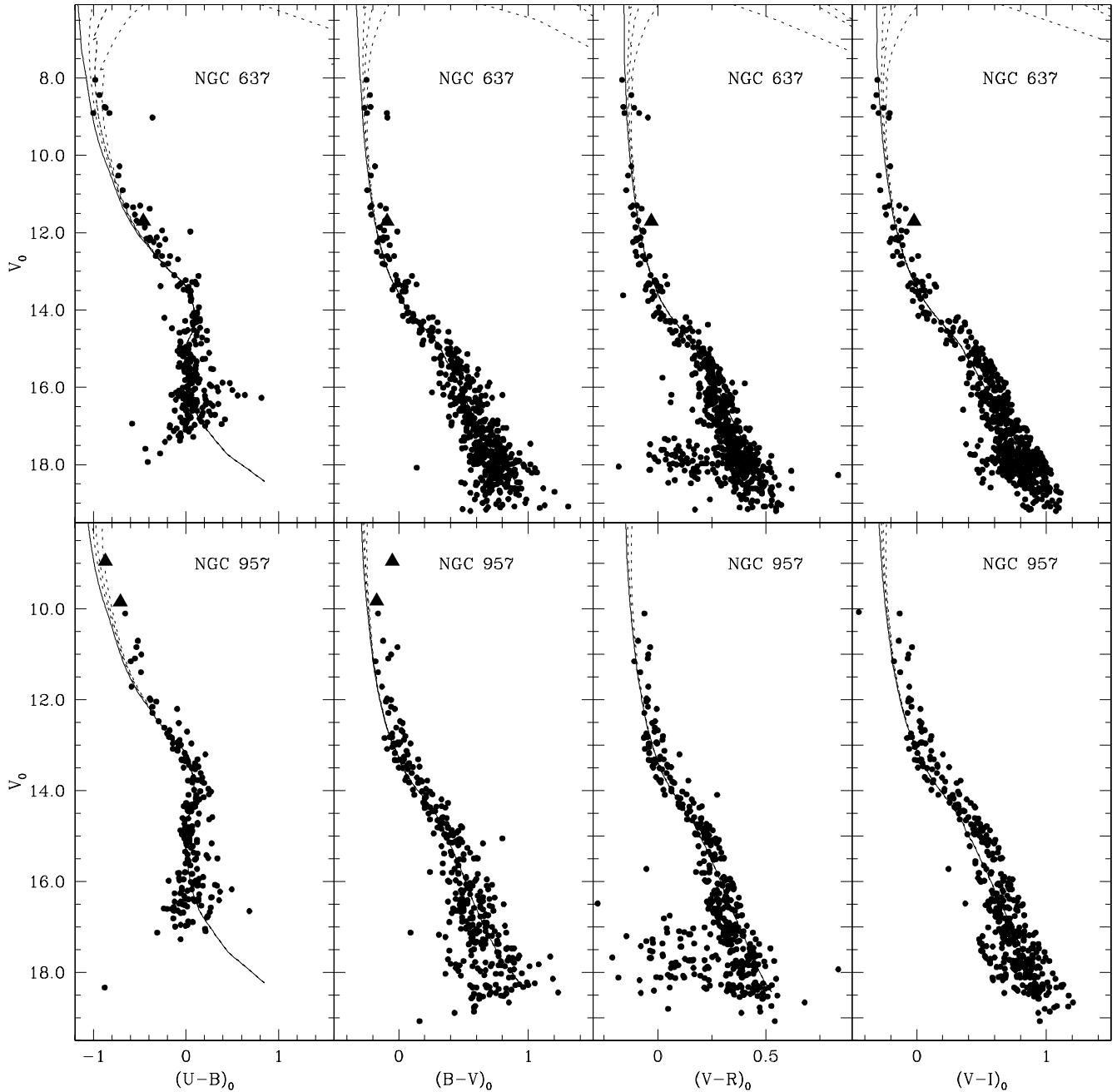


Figure 7. The plot of $(J - K)$ versus $(V - K)$ colour-colour diagram of the cluster for the stars within the cluster radius. The solid line is the ZAMS of $Z = 0.02$ fitted for the marked values of the excesses while short dash lines show the errorbars.

one using the method as described in Yadav & Sagar (2002). A theoretical ZAMS (Schaller et al. 1992) for $Z = 0.02$ is visually fitted to the blue part of intrinsic CMDs in V_0 , $(U - B)_0$, V_0 , $(B - V)_0$, V_0 , $(V - R)_0$ and V_0 , $(V - I)_0$. This gives an intrinsic distance modulus, $(m - M)_0$, of 12.0 ± 0.2 mag for NGC 637 and 11.7 ± 0.2 mag for NGC 957. The fact that we were able to find faint probable cluster members allow us to get a better definition of the cluster lower main sequence which in turn improves the estimation of the distances. The above distance moduli corresponds to a distance of 2.5 ± 0.2 kpc for NGC 637 and 2.2 ± 0.2 kpc for NGC 957. For NGC 637, it is similar to the value 2.5 kpc derived by Huestamendia et al. (1991) while it is less than the value 2.75 kpc derived by Phelps & Janes (1994). In case of NGC 957, our derived values are similar to the values given in literature (§1).

Table 5. A comparison of extinction law in the direction of cluster with normal extinction law given by Cardelli et al. (1989).

Objects	$\frac{E(U-B)}{E(V-J)}$	$\frac{E(B-V)}{E(V-J)}$	$\frac{E(V-R)}{E(V-J)}$	$\frac{E(V-I)}{E(V-J)}$	$\frac{E(V-H)}{E(V-J)}$	$\frac{E(V-K)}{E(V-J)}$	$\frac{E(J-K)}{E(V-K)}$
Normal value	0.32	0.43	0.35	0.70	1.13	1.21	0.19
NGC 637	0.32 ± 0.03	0.45 ± 0.04	0.36 ± 0.03	0.69 ± 0.05	1.11 ± 0.08	1.19 ± 0.07	0.15 ± 0.30
NGC 957	0.34 ± 0.02	0.47 ± 0.01	0.39 ± 0.03	0.75 ± 0.05	1.12 ± 0.03	1.19 ± 0.02	0.14 ± 0.30

**Figure 8.** The intrinsic colour-magnitude diagram of the clusters. The continuous solid lines curve are the ZAMS given by Schaller et al. (1992) for $Z = 0.02$ and the dotted lines are isochrones of $\log(\text{age}) = 6.8, 7.0$ and 7.2 (shown left to right respectively) for NGC 637 and NGC 957.

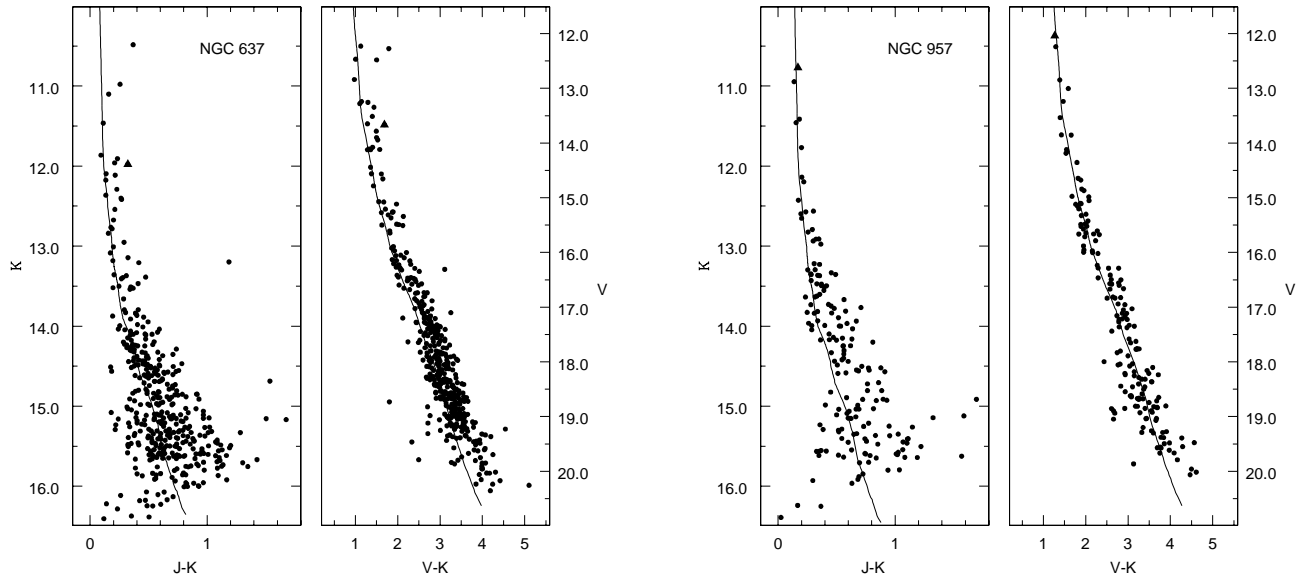


Figure 9. The K versus $(J - K)$ and V versus $(V - K)$ CMDs of the clusters using probable cluster members. The solid curve represents the isochrones of $\log(\text{age}) = 7.0$ for NGC 637 and NGC 957 taken from Schaller et al. (1992) for $Z = 0.02$.

3.7 Age of the clusters

Age of the cluster is determined by visually fitting the theoretical stellar evolutionary isochrones (Schaller et al. 1992) for $Z = 0.02$ with the observed intrinsic CMDs of the clusters as shown in Fig. 8. We chose to use the isochrones of $Z = 0.02$, as the present target clusters are young and also many recent studies, for example, by Twarog et al. (1997), does indicate that between 6.5 to 10 kpc galactocentric zone, the metallicity shows no gradient and its value is consistent with the solar value within the uncertainties. Also for cluster NGC 637, Phelps & Janes (1994) considered solar metallicity.

Isochrones of $\log(\text{age}) = 6.8, 7.0$ and 7.2 are shown with dotted lines from left to right in Fig. 8 and these visually fitted isochrones to the brighter stars indicate that CMDs are represented well with an isochrone of about 10 Myr for both the clusters. Furthermore, the isochrones of $\log(\text{age}) = 6.8$ and 7.2 Myr seem to confine blue and red end of the upper main sequence stars. The most massive stars in NGC 637 and NGC 957 is about $13 M_{\odot}$ and it sets an upper limit of about 15 Myr for the MS age of the clusters. We have therefore adopted a mean age of 10 Myr with an uncertainty of about 5 Myr for both the clusters.

The present age estimate for NGC 637 is not too different from the values of 15 Myr as derived by Huestamendia et al. (1991) and 4 Myr by Phelps & Janes (1994). For NGC 957, Gerasimenko (1991) has given an age of 5 Myr, which agrees within error with the present estimate.

Using optical and near-IR data we re-determined distance and age of both the clusters. We plot V versus $(V - K)$ and K versus $(J - K)$ CMDs in Fig 9. The theoretical isochrones given by Schaller et al. (1992) for $Z = 0.02$

and $\log(\text{age}) = 7.0$ have been overplotted in the CMDs of NGC 637 and NGC 957. The apparent distance moduli $(m - M)_{V,(V-K)}$ and $(m - M)_{K,(J-K)}$ turn out to be 14.0 ± 0.3 and 12.0 ± 0.3 mag for the cluster NGC 637 and 14.0 ± 0.3 and 12.1 ± 0.3 mag for the cluster NGC 957. Using the reddening values estimated in §3.4, we derived a distance of 2.5 ± 0.3 for NGC 637 and 2.2 ± 0.3 kpc for NGC 957. Both age and distance determination for the clusters are thus in agreement with the estimates using optical data. However, scattering is larger due to the large errors in JHK mags.

3.8 Gaps in the main-sequences

A peculiarity that appears in the intrinsic CMDs is the presence of gaps in the MS (see Fig. 8). A MS gap is present between $9 < V_0 < 10$ ($11 < M/M_{\odot} < 8$) in NGC 637. This gap has already been noticed by Huestamendia et al. (1991) and Phelps & Janes (1993). The deficiency of stars between $11 < V_0 < 12$ ($4 < M/M_{\odot} < 3$) is also seen in NGC 957. To check the significance of the gap, we computed the probability that a lack of stars in the mass interval is a result of random processes (see Scalo 1986; Giorgi et al. 2002) by using the relation $P_{\text{gap}} = (M_{\text{sup}}/M_{\text{inf}})^{(-N \times x)}$, where M_{sup} and M_{inf} are the upper and lower masses of the gap and x is the exponent of mass function while N is the number of cluster members located above the gap. Adopting the MF slope in advance (§4), we find $P_{\text{gap}} = 4\%$ for NGC 637 and 16% for NGC 957. The low resulting probabilities for both the clusters suggest that gaps in the MS are not due to the random processes. Hence, observed gaps in the MS of the clusters are real features, though we note that the significance test of gaps in MS are only approximate because the terms of the test were set after the data were observed. Specifically, upper and lower masses of the gap were derived after seeing

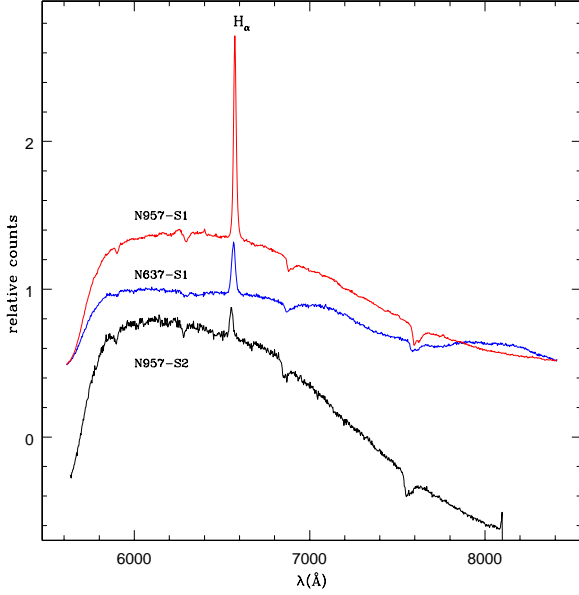


Figure 10. Slitless spectra of three emission line stars in NGC 637 and NGC 957

the data. Thus, the quantitative statistical significance of the gaps has been overestimated.

There are many reports about the MS gaps of other star clusters in the literature (Mermilliod 1976; Forbes 1996; Herbst & Miller 1982; Baume et al. 2004; Kumar et al. 2008). A detailed description of gaps in several open clusters range from the onset of convection in the stellar envelopes (Böhm-Vitense & Canterna 1974) to peculiarities in the Balmer jump and Balmer lines as suggested by Mermilliod (1976). (Ulrich 1971a,b) speculated that gaps in young clusters might be produced by the presence of ^3He isotopes that halt gravitational contraction 1-2 mags above the main-sequence. Mermilliod's gaps occur in the range of B-type stars while Böhm-Vitense & Canterna's gaps are found at less massive stars. Observed gap in NGC 637 may be related to that found by Mermilliod (1976) at the types B1-B2.

3.9 Emission type stars

The Be star phenomenon in young open clusters is known to arise due to mass loss from early type stars during its evolution on the MS and are found to be maximum for clusters with 10-25 Myr age (Fabregat & Torrejón 2000). About 20% of the early-type ($< B5$) stars show Be phenomenon in young clusters of our Galaxy (Maeder et al. 1999). However, in some young clusters, resulting from on-going/episodic star formation, an over-abundance of Be stars ($> 30\%$) are caused due to presence of Herbig Be stars, which are usually associated with nebosity and show large near-infrared excess (Subramaniam et al. 2005, 2006).

In the slit-less spectra, the emission-line stars are usu-

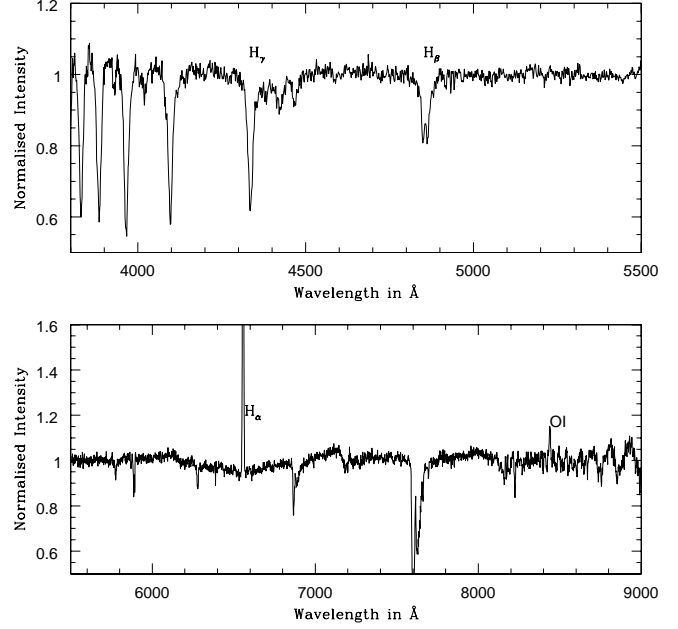


Figure 11. The normalised, continuum fitted spectra of the emission star NGC 637-S1 in the wavelength range 3700-9000 Å in the cluster NGC 637.

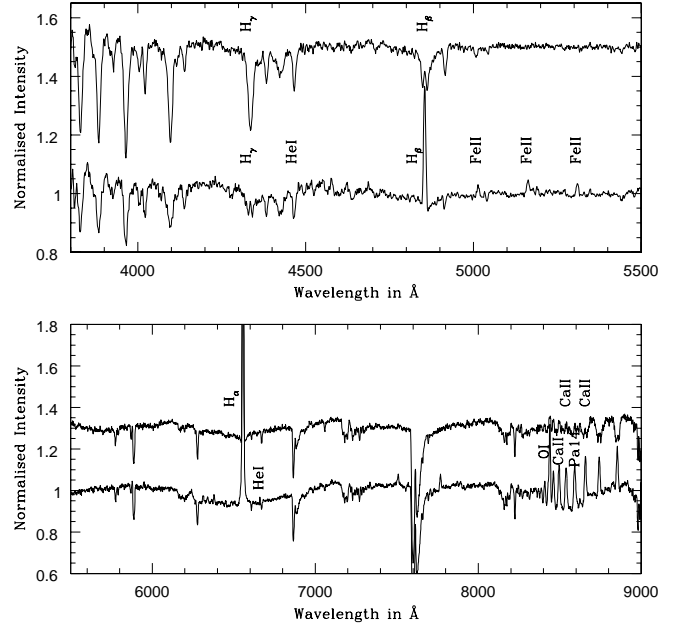


Figure 12. The normalised, continuum fitted spectra of the emission stars in NGC 957 in the wavelength range 3700-9000 Å. The top spectra corresponds to star NGC 957-S2 and the bottom one corresponds to star NGC 957-S1.

ally seen as continuum enhancement and they were identified by visual inspection of each spectra. We could identify emission-line stars with a typical limit of about $V \sim 16$ mag in 10-min exposure. This roughly corresponds to a late F-type star for present clusters. The positions of the emission stars are identified from the R -band images and the spectra are extracted from the slit-less spectral images. The spectra of individual stars are extracted with an aperture width of about 5 pixels (see Subramaniam et al. 2005, 2006, for detailed description). We identified an emission line star in NGC 637 for the first time. We also identified two emission stars in NGC 957, which are previously known. The slitless spectra of one star in NGC 637 and two stars in NGC 957 are shown in Fig. 10. These spectra cannot be used for quantitative analysis, therefore, we obtained the slit spectra of the identified emission stars. The slit spectra of NGC 637-S1 is shown in Fig. 11. The spectra show H_α in emission, H_β in emission within absorption. Two emission stars in NGC 957 were also observed in the slit mode, the spectra are shown in Fig. 12. NGC 957-S1 is found to show H_α , H_β and H_γ , along with a large number of FeII, OI and Paschen lines in emission. NGC 957-S2 shows partially filled up H_β , faint emissions in Paschen lines along with H_α emission. Photometric data with position of all three emission stars identified in the present study are listed in Table 6. Because of the CCD saturation in the present observations, photometric data of two emission stars in NGC 957 are taken from Hoag et al. (1961) and tabulated in Table 6. Thus, in the CMDs, the brighter and redder star is S1 and the fainter and bluer star is S2. The values of H_α equivalent width, stellar rotation, $v \sin i$, as estimated from the width of the HeI (4471Å) line and the disk rotation, as estimated from the width of the H_α profile are also tabulated.

The spectral type of the star is estimated from its V and $(B - V)$ magnitudes and using the estimated cluster reddening and distance. In NGC 637, the emission star is found to be a late B-type (B6.5V; NGC 637-S1) star with low infrared excess. This star is located well below the turn-off. The stellar $v \sin i$ is found to be very large, 450 km s^{-1} and disk $v \sin i$ is found to be much smaller, 180 km s^{-1} . Thus, this is a Classical Be star in the MS evolutionary phase and with large stellar rotation. Thus, this young clusters houses a fast rotating Classical Be star.

The stars NGC 957-S1 and NGC 957-S2 in the cluster NGC 957 were earlier identified by Kohoutek & Wehmeyer (1999) as emission type stars. The emission stars are found to belong to early B-type (S1 - B2V and S2 - B2.5V) from photometry. These stars are located near the tip of the cluster MS, but below the turn-off. These stars have stellar $v \sin i$ more than 300 km s^{-1} indicating these are Classical Be candidates. These stars also have low near-infrared excess which supports the above. The star with relatively large H_α emission, S1, is found to have a relatively slow rotating disk. Thus, this is another young cluster which houses Classical Be stars.

4 LUMINOSITY AND MASS FUNCTION

To construct the luminosity function for the cluster, we used the deepest V versus $(V - I)$ CMD. Photometric criteria (see §3.2) have been used to select the cluster members. The

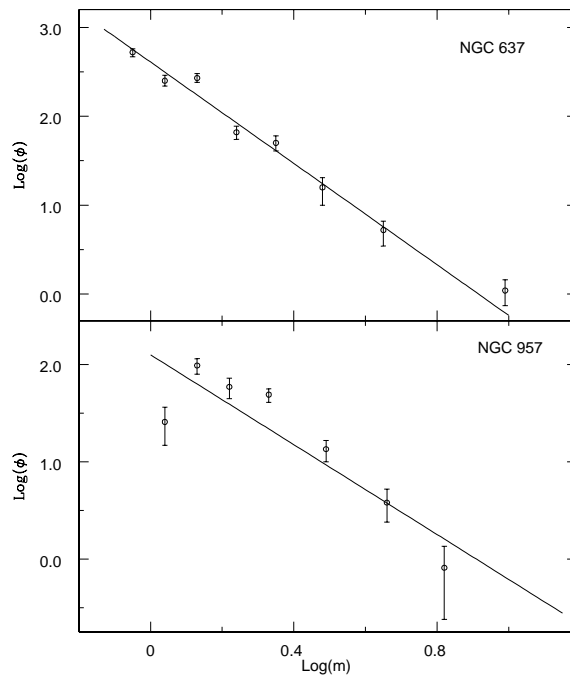


Figure 13. Mass function for NGC 637 and NGC 957 derived using Schaller et al. (1992) isochrones.

same envelope as made for selection of cluster members is also drawn in the V versus $(V - I)$ CMD of the field region (see Fig 5). Stars are counted within this envelope, for both cluster and field region. Difference between the counts in two fields after accounting for the difference in area between the cluster and field regions will be the observed cluster luminosity function. To get the correct luminosity function it is very essential to derive completeness factor of CCD data. To know about the completeness of our photometric data, we performed experiments with artificial stars using ADDSTAR routine in DAOPHOT II. Detailed description about the experiment is given in Yadav & Sagar (2002) and Sagar & Griffiths (1998). The completeness factors derived in this way are tabulated in Table 7 for NGC 637 and NGC 957 and it shows that the completeness factor is $\sim 93\%$ at 20 mag for both clusters. The completeness factor of field region is assumed to be 100%.

Using the cluster's parameters derived in this analysis and theoretical models given by Schaller et al. (1992) we have converted LF to MF and the resulting MF is shown in Fig. 13. The mass function slope can be derived by using the relation $\log \frac{dN}{dM} = -(1 + x) \times \log(M) + \text{constant}$, where dN represents the number of stars in a mass bin dM with central mass M and x is the slope of MF. The slope of the MF is $x = 1.65 \pm 0.20$ and 1.31 ± 0.50 for the cluster NGC 637 and NGC 957 respectively. Our derived values of mass function slope is in agreement within the error with the value 1.35 given by Salpeter (1955) for field stars in solar neighbourhood.

There are many MF studies available in the literature using open star clusters in the Milky Way. Recently, Piskunov et al. (2004) studied 5 young open star clusters and found that stellar mass spectra of these clusters are well represented with a power law very similar to Salpeter

Table 6. Photometric information about emission stars. Photometric data of NGC 957-S1 and NGC 957-S2 star are taken from Hoag et al. (1961).

Objects	Coordinate (J2000)	V	(U - B)	(B - V)	(V - R)	(V - I)	H α EW	vsini(disk)	vsini(star)
NGC 637-S1	$\alpha = 01^h 43^m 23^s.1$ $\delta = 64^{\circ} 01' 19''.2$	13.67	-0.03	0.55	0.38	0.78	-21.97	179.65	450.37
NGC 957-S1	$\alpha = 02^h 33^m 08^s.2$ $\delta = 57^{\circ} 28' 10''.8$	11.13	-0.38	0.66			-37.99	184.32	342.72
NGC 957-S2	$\alpha = 02^h 33^m 10^s.5$ $\delta = 57^{\circ} 32' 53''.9$	11.99	-0.28	0.54			-16.96	251.62	308.85

Table 7. Variation of completeness factor (CF) in the V, (V - I) diagram with the MS brightness.

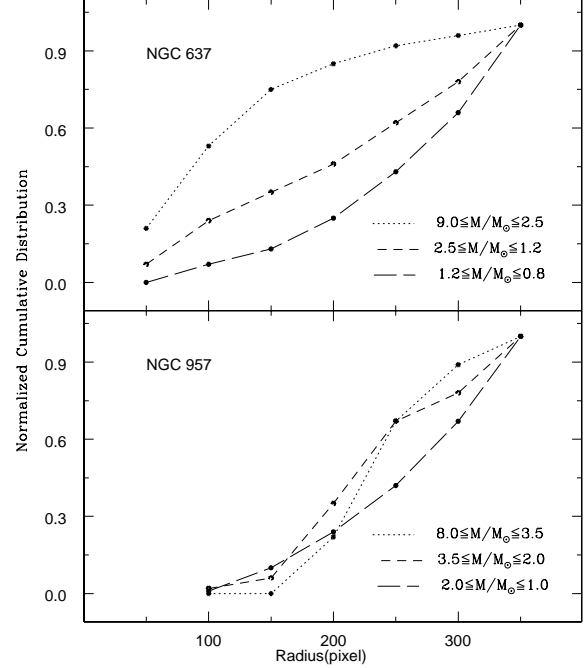
V mag range	NGC 637	NGC 957
12 - 13	0.99	0.99
13 - 14	0.99	0.99
14 - 15	0.99	0.99
15 - 16	0.98	0.98
16 - 17	0.97	0.98
17 - 18	0.95	0.94
18 - 19	0.94	0.94
19 - 20	0.93	0.93

value within the uncertainties. MF study of Phelps & Janes (1993) using a sample of seven star clusters also conclude the Salpeter type MF slope in these clusters. These studies alongwith the others (Sanner & Geffert 2001; Sagar et al. 2001; Yadav & Sagar 2002, 2004) found their results consistent with the Salpeter value.

5 MASS SEGREGATION

In order to study the mass segregation effect in the clusters, we plot the cumulative radial stellar distribution of stars for different masses in Fig 14 and mass segregation effect is seen for both the clusters, meaning, higher-mass stars gradually sink towards the cluster center than the lower mass stars. Further, We performed K-S test to see the statistical significance of mass segregation. For NGC 637, we divided the MS stars in three magnitude range i.e. $12.0 \leq V < 15.0$, $15.0 \leq V < 18.0$ and $18.0 \leq V < 20.0$ corresponding to the mass range of $9.0 \leq M/M_{\odot} < 2.5$, $2.5 \leq M/M_{\odot} < 1.2$ and $1.2 \leq M/M_{\odot} < 0.8$. For NGC 957, the magnitude range are $12.0 \leq V < 14.0$, $14.0 \leq V < 16.0$ and $16.0 \leq V < 18.0$ corresponding to the mass range of $8.0 \leq M/M_{\odot} < 3.5$, $3.5 \leq M/M_{\odot} < 2.0$ and $2.0 \leq M/M_{\odot} < 1.0$. The K-S test shows the mass segregation effect at confidence level of 99% for NGC 637 and 70% for NGC 957.

Mass segregation effect can be due to dynamical evolution or imprint of star formation or both. In the lifetime of star clusters, encounters between its member stars gradually lead to an increased degree of energy equipartition throughout the clusters. In this process the higher mass cluster members gradually sink towards the cluster center and transfer their kinetic energy to the more numerous lower-mass stellar component, thus leading to mass segregation. The time scale on which a cluster will have lost all traces of its ini-

**Figure 14.** The cumulative radial distribution of stars in various mass range.

tial conditions is well represented by its relaxation time T_E , which is given by

$$T_E = \frac{8.9 \times 10^5 N^{1/2} R_h^{3/2}}{\langle m \rangle^{1/2} \log(0.4N)} \quad (2)$$

where N is the number of cluster members, R_h is the half-mass radius of the cluster and $\langle m \rangle$ is the mean mass of the cluster stars (Spitzer & Hart 1971). The value of R_h has been assumed as half of the cluster radius derived by us. Using the above relation we estimated the dynamical relaxation time $T_E = 10$ Myr for NGC 637 and NGC 957. This indicates that the age of both clusters is same as its relaxation age. Therefore, we conclude that both the clusters are dynamically relaxed.

6 CONCLUSIONS

We studied two open star clusters NGC 637 and NGC 957 using *UBVRI* CCD and 2MASS *JHK* data. Results obtained in the analysis are the following.

- (i) The radii of the clusters are obtained as 4'2 and 4'3

which corresponds to 3.0 and 2.8 pc respectively at the distance of the clusters NGC 637 and NGC 957.

(ii) From the two colour diagram, we estimated $E(B - V) = 0.64 \pm 0.05$ mag for NGC 637 and 0.71 ± 0.05 mag for NGC 957. The JHK data in combination with the optical data provide $E(J - K) = 0.23 \pm 0.20$ mag and 0.23 ± 0.20 mag while $E(V - K) = 1.70 \pm 0.20$ mag and $E(V - K) = 2.00 \pm 0.20$ mag for NGC 637 and NGC 957 respectively. Analysis indicates that interstellar extinction law is normal towards the direction of both the clusters.

(iii) Distances to the cluster NGC 637 and NGC 957 are determined as 2.5 ± 0.2 and 2.2 ± 0.2 kpc respectively. These distances are supported by the distance values derived using optical and near-IR data. An age of 10 ± 5 Myr is determined for both NGC 637 and NGC 957 by comparing the isochrones of $Z = 0.02$ given by Schaller et al. (1992).

(iv) We discovered one emission type star in NGC 637. Two emission type stars in NGC 957 are also confirmed by the present study. These are classical Be star candidates. The two emission stars in NGC 957 are about to leave the MS while the emission star in NGC 637 is in the MS evolutionary phase.

(v) The mass function slopes $x = 1.65 \pm 0.20$ and 1.31 ± 0.50 are derived for NGC 637 and NGC 957 by considering the corrections of field star contamination and data incompleteness. Our analysis indicate that both the cluster are dynamically relaxed and one plausible reason of this relaxation may be the dynamical evolution of the clusters.

ACKNOWLEDGMENTS

We thank the anonymous referee for the useful comments and suggestions which surely helped to improve the paper. One of us (BK) acknowledge support from the Chilean center for Astrophysics FONDAP No. 15010003. This publication made use of data from the Two Micron All Sky Survey, which is a joint project of the University of Massachusetts and the Infrared Processing and Analysis Center/California Institute of Technology, funded by the National Aeronautics and Space Administration and the National Science Foundation. We are also much obliged for the use of the NASA Astrophysics Data System, of the Simbad database (Centre de Donn es Stellaires-Strasbourg, France) and of the WEBDA open cluster database.

REFERENCES

- Maeder A., Grebel E. K., Mermilliod J. C., 1999, *A&A*, 346, 459
- Baume G., Moitinho A., Giorgi E. E., Carraro G., Vazquez R. A., 2004, *A&A*, 417, 961
- Bessell, M. S., 1979, *PASP*, 91, 589
- B hm-Vitense E., Canterna R., 1974, *ApJ*, 194, 629
- Caldwell A. R., John, Cousins, A. W. J., Ahlers C. C., Wamelen P. van, Maritz E. J., 1993, *SAAO Circ. No. 15*
- Cardelli J. A., Clayton G. C., Mathis J. S., 1989, *ApJ*, 345, 245
- Dias W. S., Alessi B. S., Moitinho A., L pine J. R. D., 2002, *A&A*, 389, 871
- Fabregat J., Torrej n J.M., 2000, *A&A*, 357, 451
- FitzGerald M. P., 1970, *A&A*, 4, 234
- Forbes D., 1996, *AJ*, 112, 1073
- Gerasimenko T. P., 1991, *Astron. Zh*, 68, 1103
- Jimenez A., Garcia-pelayo J., 1980, *A&AS*, 41, 9
- Giorgi E. E., Vazquez R. A., Baume G., Seggewiss W., Will J.-M., 2002, *A&A*, 381, 884
- Grubisich C., 1975, *A&AS*, 21, 99
- Hoag A. A., Johnson H. L., Iriarte B., Mitchell R. I., Hallam K. L., Sharpless S., 1961, *Publ. US. Nav. Obs.* 17, 347
- Huestamendia G., del Rio G., Mermilliod J.-C., 1991, *A&AS*, 87, 153
- Herbst W. & Miller D. P., 1982, *AJ*, 87, 1478
- Johnson H. L., Morgan W. W., 1953, *ApJ*, 117, 313
- Johnson H. L., Morgan W. W., 1966, *ARA&A*, 4, 193
- King, Ivan, 1962, *AJ*, 67, 274
- Kohoutek L., Wehmeyer R., 1999, *A&AS*, 134, 255
- Koornneef J., 1983, *A&A*, 128, 84
- Kumar B., Sagar R., Melnick J., 2008, *MNRAS*, 386, 1380
- Landolt A. U., 1992, *AJ*, 104, 340
- Mermilliod J.-C., 1976, *A&A*, 53, 289
- Persson S. E., Murphy D. C., Krzeminski W., Roth M., Rieke M. J., 1998, *AJ*, 116, 2475
- Phelps R. L., Janes K. A., 1993, *AJ*, 106, 1870
- Phelps R. L., Janes K. A., 1994, *ApJS*, 90, 31
- Piskunov A. E., Belikov A. N., Kharchenko N. V., Sagar, R., Subramaniam A., 2004, *MNRAS*, 349, 1449.
- Rachford B. J., Canterna R., 2000, *AJ*, 119, 1296
- Ruprecht J., 1966, *Bull. astr. Inst. Czechosl.*, 17, 33
- Sagar R., Griffiths W. K., 1998, *MNRAS*, 299, 777
- Sagar R., Munari U., de Boer K. S., 2001, *MNRAS*, 327, 23
- Salpeter E. E., 1955, *ApJ*, 121, 161
- Sanner J., Geffert M., 2001, *A&A*, 370, 87
- Scalo J. M., 1986, *Fund. Cosmic Phys.*, 11, 1
- Schaller G., Schaerer D., Meynet G., Maeder A., 1992, *A&AS*, 96, 269
- Schmidt - Kaler Th., 1982, In: Landolt/Bornstein, Numerical Data and Functional Relationship in Science and Technology, New series, Group VI, Vol. 2b, Scaifers K. & Voigt H. H. (eds.) Springer - Verlag, Berlin, p. 14
- Spitzer L., Hart M. H., 1971, *ApJ*, 164, 399
- Stetson P. B., 1987, *PASP*, 99, 191
- Stetson P. B., 1992, in Warrall D. M., Biemesderfer C., Barnes J. eds., *ASP Conf. Ser. Vol. 25, Astronomical Data Analysis Software and System I. Astron. Soc. Pac., San Francisco*, p. 297
- Subramaniam A., Sahu D. K., Sagar R., Vijitha P., 2005, *A&A*, 440, 511
- Subramaniam A., Mathew, B., Bhatt, B. C., Ramya S., 2006, *MNRAS*, 370, 743
- Twarog B. A., Ashman K. M., Anthony-Twarog B. J., 1997, *AJ*, 114, 2556
- Ulrich R. K., 1971a, *ApJ*, 165, L95
- Ulrich R. K., 1971b, *ApJ*, 168, 57
- Whittet D. C. B., van Breda I. G., 1980, *MNRAS*, 192, 467
- Yadav R. K. S., Sagar R., 2002, *MNRAS*, 337, 133
- Yadav R. K. S., Sagar R., 2004, *MNRAS*, 351, 667